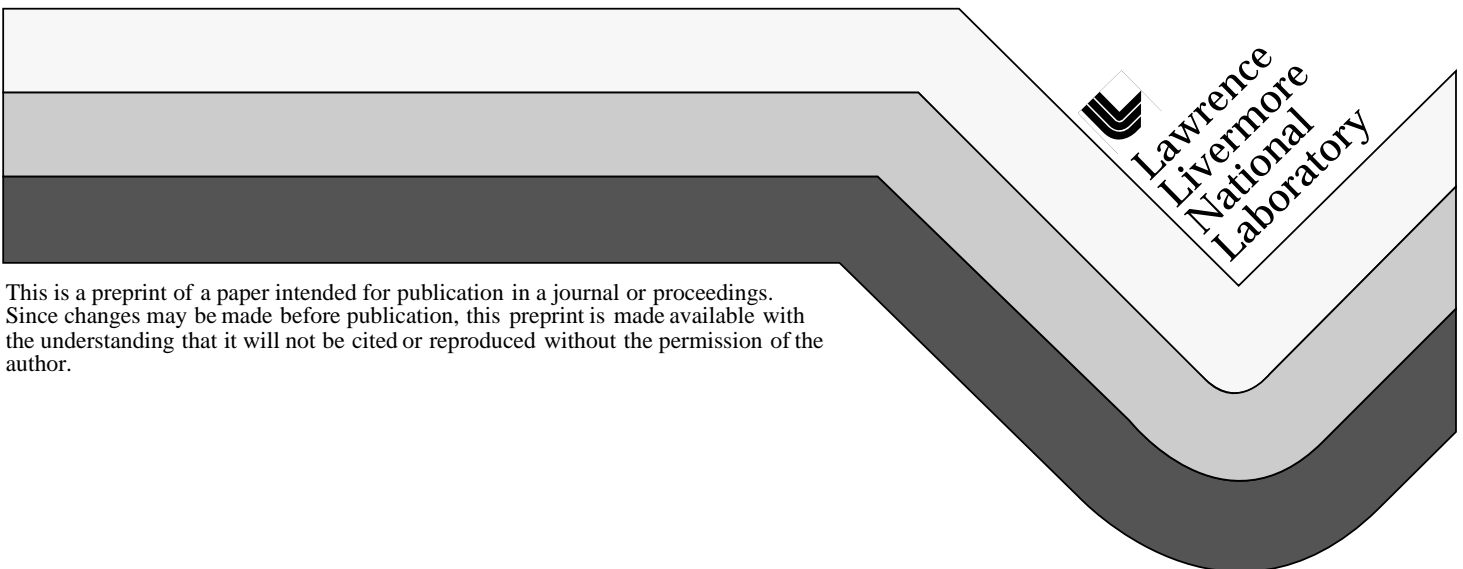# Oxidation of Automotive Primary Reference Fuels at Elevated Pressures

H.J. Curran
W.J. Pitz
C.K. Westbrook
C.V. Callahan
F.L. Dryer

Lawrence
Livermore
National
Laboratory

OXIDATION OF AUTOMOTIVE PRIMARY REFERENCE FUELS AT ELEVATED PRESSURES

H. J. CURRAN,[1] W. J. PITZ,[1] C. K. WESTBROOK,[1] C. V. CALLAHAN[2] AND F. L. DRYER[2]

[1]Lawrence Livermore National Laboratory
Livermore, CA 94551, USA
[2]Department of Mechanical and Aerospace Engineering
Princeton University
Princeton, NJ 08544, USA

Automotive engine knock limits the maximum operating compression ratio and ultimate thermodynamic efficiency of spark-ignition (SI) engines. In compression-ignition (CI) or diesel cycle engines, the premixed burn phase, which occurs shortly after injection, determines the time it takes for autoignition to occur. In order to improve engine efficiency and to recommend more efficient, cleaner-burning alternative fuels, we must understand the chemical kinetic processes that lead to autoignition in both SI and CI engines. These engines burn large molecular-weight blended fuels, a class to which the primary reference fuels (PRF) *n*-heptane and iso-octane belong. In this study, experiments were performed under enginelike conditions in a high-pressure flow reactor using both the pure PRF fuels and their mixtures in the temperature range 550–880 K and at 12.5 atm pressure. These experiments not only provide information on the reactivity of each fuel but also identify the major intermediate products formed during the oxidation process. A detailed chemical kinetic mechanism is used to simulate these experiments, and comparisons of experimentally measured and model predicted profiles for O_2, CO, CO_2, H_2O and temperature rise are presented. Intermediates identified in the flow reactor are compared with those present in the computations, and the kinetic pathways leading to their formation are discussed. In addition, autoignition delay times measured in a shock tube over the temperature range 690–1220 K and at 40 atm pressure were simulated. Good agreement between experiment and simulation was obtained for both the pure fuels and their mixtures. Finally, quantitative values of major intermediates measured in the exhaust gas of a cooperative fuels research engine operating under motored engine conditions are presented together with those predicted by the detailed model.

Introduction

Detailed kinetic mechanisms are needed to understand fully the fundamental chemical processes involved in fuel oxidation and to make intelligent recommendations for additives and replacement compounds that can be used to improve engine operating efficiency and reduce tailpipe emissions. Kinetic mechanisms must predict properly key processes controlled by chemical reactions that occur in spark-ignition (SI) and compression-ignition (CI) or diesel cycle engine combustion. In SI engines, mechanisms must predict accurately automotive engine knock that limits the maximum operating compression ratio and ultimate thermodynamic efficiency of the engine. Detailed mechanisms must also predict partial oxidation of hydrocarbons emerging from crevices, a process which leads to raw hydrocarbon emission speciation from SI engines [1,2]. In CI engines, the kinetic mechanism must accurately predict the premixed burn phase that occurs shortly after injection and determines the time required for autoignition to occur [3].

In this study, a detailed chemical kinetic mechanism has been assembled for the primary reference fuels (PRF) *n*-heptane and iso-octane, which are used to define the octane reference scale for fully blended gasolines. The chemistry of *n*-heptane and iso-octane mixtures includes many of the features of large molecular-weight blended fuels. *n*-Heptane is a reactive straight-chain paraffin while iso-octane is a less reactive branched-chain paraffin. Each fuel exhibits richly complex chemistry; at high temperatures, fuel decomposition reactions tend to dominate the combustion process, whereas at low temperatures, the chemistry is dominated by addition of alkyl radicals to O_2 and subsequent isomerization reactions. Both low- and high-temperature regimes are important for blended fuels used in SI and CI engines. However, the higher operating pressures encountered in CI engines place an even greater emphasis on the low-temperature chemistry. Ultimately, our goal is to generate a chemical kinetic mechanism to describe a "surrogate" diesel fuel. Our current surrogate fuel lacks representation of the aromatic species, which are an appreciable fraction of

RH

β-scission at high T

$\dot{R}$ $\longrightarrow$ olefin + $\dot{R}'$

O_2

$R\dot{O}_2$

olefin + $H\dot{O}_2$

$\dot{Q}OOH$ $\longrightarrow$ epoxide + $\dot{O}H$

O_2 β-scission products

$\dot{O}_2QOOH$

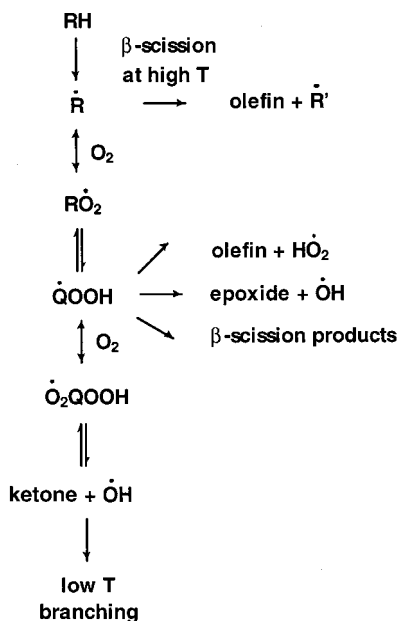ketone + $\dot{O}H$

low T branching

FIG. 1. Schematic representation of the primary oxidation reactions.

conventional diesel fuel. These components will be considered in future work.

Experimental studies of primary reference fuels have been performed in closed vessels [4], flow reactors [5,6], jet-stirred reactors [7–11], shock tubes [12,13], rapid compression machines [1,14–19] and motored engines [20–22]. Ranzi et al. [23,24] and Côme et al. [25,26] have generated reduced chemical kinetic mechanisms to describe PRF oxidation at low, intermediate, and high temperatures. Roberts et al. [27] used a semi-detailed chemical mechanism that was supplemented by adding a knock submodel to simulate iso-octane ignition in a cooperative fuels research (CFR) engine. Detailed mechanisms have also been generated automatically by Warnatz and collaborators [28–30] using rules for different reaction classes.

The PRF mechanism developed here must simulate the autoignition phenomena and intermediate product formation at the high-pressure conditions found in internal combustion engines. To attain a predictive and validated model, computed results are compared to experimental results at elevated pressures. Predictions of the detailed model are compared to ignition delay times measured in a shock tube [13] and in a high-pressure flow reactor [6]. The flow reactor studies oxidation of PRF mixtures under well-controlled, well-characterized conditions, providing valuable information on major

intermediate species formed in the oxidation process. The reaction pathways responsible for the intermediate products formed were identified, and comparisons with previous studies of the oxidation of PRF mixtures in engines [20–27] are made.

Previously, computed results from a lumped mechanism were compared to these same experimental results for major species profiles (CO, CO_2, H_2O, O_2) [6]. The agreement was very good and provided a sound validation of the lumped model where elementary reactions in the same reaction class and isomeric species are grouped together, to reduce the computational requirements compared to detailed models. In the present work, our goal is to validate a fully detailed chemical kinetic model that is more fundamentally based on elementary reactions than lumped models.

Chemical Kinetic Mechanism

Computer simulations were performed using the HCT model [31], which solves the coupled chemical kinetic and conservation equations for energy, mass, and momentum under a variety of boundary and initial conditions for reactive systems. The high-pressure reactor experiments were simulated as an adiabatic, isobaric (12.5 atm) plug flow with negligible axial diffusion of species and energy. Shock-tube simulations assumed constant volume behind a reflected shock wave. The detailed chemical kinetic reaction mechanism used in these calculations is based on previous work [32–40] and on the hierarchical nature of reacting systems starting with a core mechanism describing H_2/O_2 and CO oxidation. To this is added the progressively larger C_1–C_8 mechanisms. The complete PRF model consists of approximately 990 different chemical species and 4060 elementary reactions.

The overall flux diagram for fuel oxidation is shown schematically in Fig. 1. The naming conventions used are $\dot{R}$ and $\dot{R}'$, denoting alkyl radicals, and Q, denoting C_nH_{2n} species. At low temperatures, chain branching is mainly due to the reaction pathway leading through the ketohydroperoxide species, which forms two reactive hydroxyl radicals. As the temperature rises, chain propagation reactions of the $\dot{Q}OOH$ radical become more important, because the energy barrier associated with $\dot{Q}OOH$ scission is more easily overcome. This leads to the formation of cyclic ethers, conjugate olefins, and β-decomposition products together with only one radical species. The increasing importance of these propagation channels leads to a lower reactivity of the system, observed as a negative temperature coefficient (NTC) of reaction. At intermediate and high temperatures, the overall reaction pathway proceeds via fuel decomposition and alkyl radical β-scission, proceeding rapidly to smaller olefinic and radical
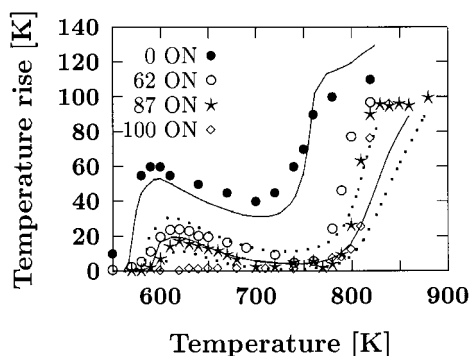
FIG. 2. PRF oxidation at 12.5 atm, $\phi = 1.0$, $\tau = 1.8$ s, 98.3% N_2. Experimental (symbols) [6] versus model-predicted temperature rise in reactor as a function of inlet reactor temperature. Dotted lines correspond to open symbols.

species. Chain branching at intermediate temperatures occurs primarily through the sequence fuel + $H\dot{O}_2 = \dot{R} + H_2O_2$ and $H_2O_2 = \dot{O}H + \dot{O}H$, and at high temperatures through the reaction $\dot{H} + O_2 = \dot{O} + \dot{O}H$.

Our most recent modeling work [40] describes how rate constant expressions are estimated for important reactions. These rate expressions rely on thermodynamic parameters for reacting species to ensure correct equilibrium balance. We employ the program THERM [41], which uses group additivity rules developed by Benson [42], to evaluate thermochemical quantities for chemical species where there are no available data. H-C-O groups and bond dissociation groups were updated, based on recent work by Bozzelli and coworkers [43]. A full listing of the reaction mechanism can be obtained by Internet electronic mail (curran6@llnl.gov) by writing to the authors.

Experimental

The Princeton variable-pressure flow reactor provides a well-characterized environment that is designed to minimize mixing and diffusion effects. Details of the apparatus have been described previously [6,44–47]. Both PRF fuels and their mixtures were studied under stoichiometric oxygen to fuel ratios, at a constant molar carbon content of 1% with nitrogen diluent of approximately 98.3%. Experiments were performed over an initial reactor temperature range of 550–850 K, and with a constant pressure and residence time of 12.5 atm and 1.8 s, respectively. In the experiments reported here, a continuous gas sampling flow was extracted from an axial location downstream of the point where a stream of prevaporized fuel diluted in nitrogen was mixed with the main carrier flow of nitrogen and the desired amount of oxygen. The sampled flow was removed and quenched utilizing a hot-water cooled, convection-quench, stainless steel sampling probe. Temperature measurements were made at the point of sample extraction using a silica-coated thermocouple. The sampled gases were passed through heated (100 °C) Teflon lines and through the following on-line analyzers: a Fourier transform infrared (FTIR) system to determine water, carbon monoxide, and carbon dioxide; an electrochemical analyzer to determine oxygen; and nondispersive infrared analyzers for carbon monoxide and carbon dioxide. To obtain identification of hydrocarbon species in the sampled gases, small amounts of gases were extracted from the sample stream and stored off-line in a heated, multiloop sample valve for analysis using gas chromatograph techniques. Species identifications were made using a DB-5 semipolar column to separate the heavy components. Identification of the chemical species present was made using an FTIR detector and comparisons between detected spectra with either spectra from known compounds or best fits against those from an existing library created at Princeton. Low-molecular-weight components were analyzed separately using a Plot Q column and flame ionization detection. Other experimental procedures were as described elsewhere [6,46].

Discussion

Figure 2 shows comparisons of the measured and simulated reactor temperature rise as a function of initial temperature for each of the two pure PRF fuels and their mixtures. Gas temperature rise results from the exothermic character of the reaction process. From 560 to 580 K initial reactor temperature, n-heptane and the PRF mixtures begin to show some conversion, with reactivity peaking from 600 to 625 K due to the decomposition of ketohydroperoxide species and the formation of a second reactive hydroxyl radical, resulting in chain-branching [23,40,48]. At lower initial temperatures, no fuel conversion is observed because ketohydroperoxide decomposition has a high activation energy barrier of approximately 43 kcal/mol. From 600 to 700 K for n-heptane and 625 to 780 K for PRF fuel mixtures, a gradual but pronounced decrease is observed in fuel conversion. This characteristic NTC behavior is common to paraffin fuel oxidation at low temperatures and is due to β-scission of $\dot{Q}OOH$ radicals, resulting in the formation of only one radical species in addition to cyclic ether, olefin, and oxygenated β-scission products. At initial reactor temperatures above 780 K, H_2O_2 dissociates into two reactive hydroxyl radicals leading to a rapid increase in system reactivity and consumption of the remaining fuel.

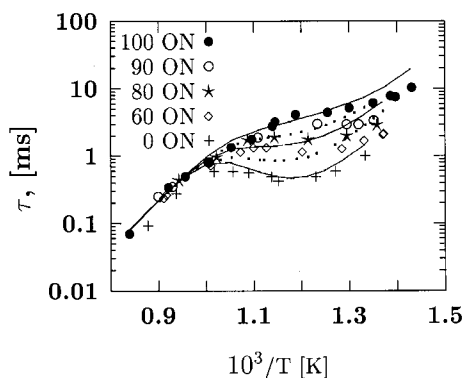It appears that H_2O_2 dissociation occurs at lower

FIG. 3. PRF oxidation at 40 atm, stoichiometric fuel in air. Experimental (symbols) [13] versus model-predicted ignition delay times. Dotted lines correspond to open symbols.
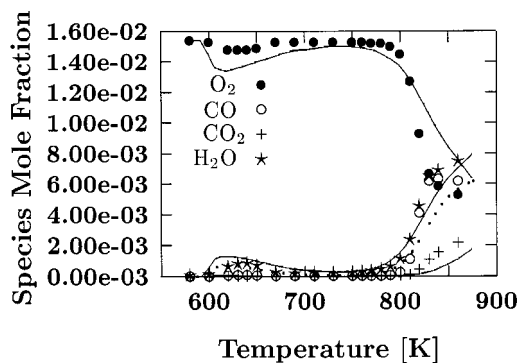

FIG. 4. 92 ON oxidation at 12.5 atm, $\phi = 1.0$, $\tau = 1.8$ s, 98.3% N_2. Experimental (symbols) [6] versus model-predicted species concentrations as a function of inlet reactor temperature. Dotted lines correspond to open symbols.

initial temperatures for n-heptane than for iso-octane and other PRF mixtures. This is because n-heptane partially reacts increasing its temperature above the initial reactor temperature. At initial temperatures above 780 K, β-scission of the larger alkyl radicals becomes increasingly important, leading to the formation of smaller olefins and alkyl radicals including methyl. At these conditions, the methyl radicals formed react primarily with hydroperoxy radicals, leading to the formation of methoxy and hydroxy radicals $\dot{C}H_3 + H\dot{O}_2 = CH_3\dot{O} + \dot{O}H$ followed by $CH_3\dot{O} + M = CH_2O + \dot{H} + M$. The formaldehyde produced undergoes further reaction, primarily via $CH_2O + \dot{R} = H\dot{C}O + RH$ and $H\dot{C}O + O_2 = CO + H\dot{O}_2$. At higher temperatures (>1100 K), the latter reaction is superceded by $H\dot{C}O + M = CO + \dot{H} + M$. This sequence of

reactions is highly exothermic and converts relatively unreactive radicals to very reactive ones.

Overall, there is good agreement between model predictions and experimentally measured temperature rise. The relative trends in fuel reactivity observed in the experiment are reproduced well by the detailed mechanism. The reactivity of n-heptane, the PRF mixtures and iso-octane, is reproduced very well by the model throughout the NTC region. However, the model predicts greater conversion of iso-octane than that observed in the experiment over the temperature range 610–660 K. At higher temperatures (780–850 K), the model predicts the onset of the hot ignition stage that is controlled by H_2O_2 decomposition but is not quite as rapid as observed in the experiments for 87 ON PRF and iso-octane.

The detailed mechanism was also used to simulate the shock-tube experiments of Fieweger et al. [13], results of which are plotted in Fig. 3. Good agreement is observed between predicted and experimental autoignition delay times for pure n-heptane and iso-octane fuels and their mixtures throughout the NTC region. Submechanisms for the two PRF fuels were found to interact only through small radical species such as $\dot{O}H$, $H\dot{O}_2$, $\dot{O}$, $\dot{H}$, and $\dot{C}H_3$. This observation supports earlier work by Lee and Morley [50] and observations by Leppard [20] and Li et al. [22].

Comparisons of predicted overall reactivity with experimental observations test the kinetic mechanism but do not validate the complex chemical processes leading to partial oxidation or autoignition. To perform a more detailed test of the model, we compare measured speciation data with that predicted by the model. Figure 4 shows comparisons of experimental measurements and model predictions for O_2, CO, CO_2, and H_2O species produced in 92 ON PRF mixture oxidation. The predictions agree with the experimental results quite well, although the computed hot ignition stage is not quite as rapid as observed in the experiment. In addition, many larger intermediates were positively identified by matching the retention times and GC-FTIR spectral peaks to those in a library. Table 1 reports these positively identified species, together with concentrations for 92 ON PRF fuel predicted by the model. All the identified species are predicted in detectable concentrations except ethane and 4-methyl-2-pentanone. We have used the output from the detailed model to discern the various intermediates formed at 640 and 820 K and have classified them by type, that is, olefins, aldehydes, ketones, and cyclic oxygenates, in Table 2. Unreacted fuel and methane constitute the paraffinic species present. The species formed in most abundance are the small C_1 oxygenates of formaldehyde, carbon monoxide and carbon dioxide. However, it is evident that the C_4 submechanism plays a large part in iso-octane oxidation under these conditions.

TABLE 1

Comparison of major intermediates positively identified by GC-FTIR and predicted by the model. 92 ON oxidation at 12.5 atm, $\phi = 1.0$, $\tau = 1.8$ s, $T = 640$ K, 1.0% carbon

92 ON PRF Intermediates	Model-Predicted Species Mole Fraction
Formaldehyde	2.87e-4
Ethane	9.04e-8
Propene	7.50e-5
Isobutene	2.34e-4
Acetone	1.56e-4
Isobuteraldehyde	2.28e-5
Methacrolein	3.90e-6
2,2-Dimethyl propanal	2.95e-5
4,4-Dimethyl-2-pentene	1.80e-6
2,4-Dimethyl-2-pentene	3.25e-6
2,4,4-Trimethyl-1-pentene	4.89e-5
2,4,4-Trimethyl-2-pentene	4.44e-5
4-Methyl-2-pentanone	2.63e-8
2,2,4,4-Tetramethyl-THF	1.02e-4

TABLE 2

Model-predicted mole fractions of major intermediates produced in a flow reactor. 92 ON oxidation at 12.5 atm, $\phi = 1.0$, $\tau = 1.8$ s, 1.0% carbon

Predicted Species Formed	Reactor Temperature	
	640 K	820 K
Olefin		
Propene	7.50e-5	3.59e-4
Isobutene	2.34e-4	5.48e-4
2-Methyl-1-pentene	3.58e-6	8.30e-6
2,4-Dimethyl-1-pentene	8.94e-7	8.80e-6
2,4-Dimethyl-2-pentene	3.25e-6	6.87e-5
4,4-Dimethyl-1-pentene	2.36e-6	4.43e-5
4,4-Dimethyl-2-pentene	1.80e-6	1.19e-5
2,4,4-Trimethyl-1-pentene	4.89e-5	2.61e-6
2,4,4-Trimethyl-2-pentene	4.44e-5	1.34e-5
Aldehyde		
Formaldehyde	2.87e-4	4.82e-4
Acetaldehyde	3.58e-5	1.77e-5
Isobuteraldehyde	2.28e-5	1.62e-5
Methacrolein	3.90e-6	8.19e-6
Pentanaldehyde	2.67e-6	—
2,2-Dimethyl propanal	2.95e-5	—
Ketone		
Acetone	1.56e-4	8.12e-5
2-Pentanone	6.48e-6	—
4-Methyl-2-pentanone	2.63e-8	—
2,4-Dimethyl-3-pentanone	6.89e-6	—
2,2-Dimethyl-3-pentanone	3.74e-6	—
4,4-Dimethyl-2-pentanone	1.51e-6	—
Cyclic Ether		
2-Methyl oxirane	1.86e-6	2.86e-5
Isobutene oxide	3.42e-6	6.73e-5
2,4,4-Trimethyl-THF	1.85e-6	—
2-Propyl-THF	1.87e-6	—
2-Methyl,5-ethyl-THF	4.23e-6	1.37e-6
2,2,4,4-Tetramethyl-THF	1.02e-4	1.31e-6
2-t-Butyl-3-methyl-oxetane	3.81e-6	—
2-Isopropyl-3,3-dimethyl-oxetane	3.77e-6	—

Leppard [20] performed autoignition experiments in a CFR engine motored at 500 RPM using *n*-heptane, iso-octane, and PRF mixtures and speciated the exhaust gases. With an intake manifold pressure of 120 kPa and temperature of 448 K, iso-octane autoignited at a critical compression ratio (CCR) of 10.7, while at a compression ratio (CR) of 10.5, autoignition was not observed, although 36% of the fuel had reacted. The model predicts a CCR of 10.25 with 44.5% of the fuel oxidized. Table 3 shows experimental results together with those predicted by the detailed mechanism, both at 36% fuel conversion. Isobutene was the largest measured alkene component by a factor of 5, with propene and di- and tri-methyl pentenes composing the remainder. The model predicts isobutene formation in greatest abundance, but propene is overpredicted by a factor of 3. Of the pentenes, the predicted concentrations of 2,4-dimethyl-2-pentene, 2,4,4-trimethyl-1-pentene, and 2,4,4-trimethyl-2-pentene are quite good even though the relative concentrations of the trimethyl pentenes are reversed. In addition, 4,4-dimethyl-2-pentene is underpredicted by about an order of magnitude.

The only alkanes identified were methane (in trace amounts) and iso-octane. Of the measured oxygenates, formaldehyde, 2,2,4,4-tetramethyl-tetrahydrofuran (TMTHF), and acetone were present in the greatest amounts, followed by 2-tert-butyl-3-methyl oxetane, 2-isopropyl-3,3-dimethyl oxetane, isobuteraldehyde, and methacrolein. Formaldehyde is predicted within a factor of 2, while acetone is overpredicted by about an order of magnitude. TMTHF is

underpredicted by less than a factor of 3, and the oxetanes are also underpredicted by almost an order of magnitude. Isobuteraldehyde is in good agreement, but the model underpredicts methacrolein by about a factor of 3. The prediction of intermediate speciation data measured in engine experiments is extremely difficult, as the system passes through a wide range of temperatures and pressures within the engine, and the exhaust flow that is analyzed here is also unsteady. We believe that overall, good agreement is observed between model prediction and

Iso-octane Intermediates	Species Mole Fraction	
	Experiment	Model Prediction
Carbon monoxide	2.310e-3	3.29e-3
Isobutene	1.694e-3	3.72e-3
Formaldehyde	1.170e-3	2.89e-3
2,2,4,4-Tetramethyl-THF	1.011e-3	3.82e-4
Acetone	8.180e-4	8.65e-3
2-t-Butyl-3-methyloxetane	5.510e-4	1.85e-5
2-Isopropyl-3,3-dimethyloxetane	4.740e-4	5.16e-5
Propene	3.230e-4	1.09e-3
4,4-Dimethyl-2-pentene	2.520e-4	3.45e-5
2,4,4-Trimethyl-1-pentene	2.320e-4	5.14e-4
Isobuteraldehyde	2.070e-4	3.11e-4
Methacrolein	1.860e-4	6.57e-5
2,4-Dimethyl-2-pentene	1.680e-4	1.49e-4
2,4,4-Trimethyl-2-pentene	1.520e-4	5.49e-4
2,3-Epoxy-2,4,4-trimethylpentane	1.430e-4	1.11e-5
Isobutene oxide	1.390e-4	1.02e-4
2,2-Dimethyl propanal	1.300e-4	2.34e-4

experimental observation, although some refinements may be possible in the chemistry.

Li et al. [22] also studied iso-octane autoignition in a motored, single-cylinder engine and obtained in-cylinder samples at different points prior to autoignition. They found that, compared to n-heptane, iso-octane showed considerably less reactivity with very little reaction until about 10° BTDC and that isobutene and TMTHF were the major intermediates formed during iso-octane oxidation in agreement with Leppard's experiments. In addition, the di- and tri-methyl pentenes were also observed, as were the C_1 to C_4 aldehydes and C_8 oxetane species. 2,2-Dimethyl propanal was also detected in trace amounts.

The present model identifies the major intermediate species important for PRF oxidation in engines. In the following section, we use the modeling results to identify the reaction pathways that lead to their formation in the high-pressure flow reactor.
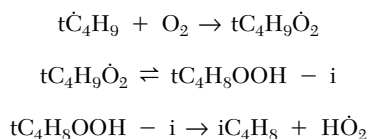
Olefin Formation

Computed results indicate that, at both 640 and 820 K, the only possible C_8 olefins are 2,4,4-trimethyl-1-pentene and 2,4,4-trimethyl-2-pentene which are produced from the decomposition of the corresponding hydroperoxyl-alkyl radical, for example, 2-methylhydroperoxyl-4,4-dimethyl-pent-2-yl radical

produces 2,4,4-trimethyl-1-pentene and hydroperoxyl radical.

At 640 K, the C_7 olefins are formed primarily from C_8 hydroperoxy-alkyl β-scission and from C_8 cyclic ether oxidation with a small proportion of 4,4-dimethyl-2-pentene generated from β-scission of 2,4,4-trimethyl-pent-3-yl radical. Higher concentrations of C_7 olefins are formed at 820 K, mainly from the decomposition of C_8 alkyl radicals.

The olefinic species predicted in highest concentration is isobutene, whereas isobutene oxygenates are also predicted in relatively high concentrations by the model. Analysis of reaction path edits at both 640 and 820 K indicates that isobutene is formed primarily via β-scission of 2,4,4-trimethyl-pent-1-yl (octyl) radical to form isobutene and tert-butyl radical. The tert-butyl radicals also produce isobutene via the following sequence:

$$t\dot{C}_4H_9 + O_2 \rightarrow tC_4H_9\dot{O}_2$$

$$tC_4H_9\dot{O}_2 \rightleftharpoons tC_4H_8OOH - i$$

$$tC_4H_8OOH - i \rightarrow iC_4H_8 + H\dot{O}_2$$

A small quantity of isobutene is also formed from β-scission of 2,4,4-trimethyl-pent-5-yl radical to produce isobutene and isobutyl radical, and the 2,4,4-trimethyl-3-hydroperoxy-pent-5-yl radical scission to yield isobutene, isobuteraldehyde, and hydroxyl radical.

At 640 K, because of the high-energy barrier for β-scission, one expects that only addition of alkyl radicals to O_2 will occur, a behavior we observe in n-heptane oxidation [40]. The A-factor of a reaction is proportional to $e^{\Delta S/R}$, where ΔS is the entropy change from reactants to products. The entropy change for iso-octyl is greater than for n-heptyl β-scission reactions, and this results in higher A-factors for iso-octyl β-decompositions. This is an important feature captured by the detailed mechanism, because β-scission of iso-octyl radicals at this temperature will result in less chain branching and thus lower reactivity of the system relative to n-heptane oxidation under the same conditions. Other effects, such as the relative rate of alkylperoxyl radical isomerization, may also contribute to the experimentally observed reduction in reactivity for iso-octane relative to n-heptane. The reduced mechanisms of Ranzi et al. [23,24] and Côme et al. [25,26] consider only one generic alkyl radical β-scission reaction (in the forward, endothermic direction) for iso-octane and n-heptane assuming that the rate constant is similar for both straight-chained and branched hydrocarbons. In the detailed mechanism, the rate constants for each individual β-scission reactions are estimated in the better-known reverse, exothermic direction for the addition of an alkyl radical to an olefin with the forward rate calculated from thermochemistry.

Oxygenate Formation

The only C_8 oxygenated species observed in experiments and predicted by the model are cyclic ethers. High concentrations of TMTHF were observed and are predicted in addition to lower concentrations of 2-*t*-butyl-3-methyloxetane and 2-isopropyl-3,3-dimethyloxetane. These species are formed from the β-scission of the corresponding C_8 hydroperoxy-alkyl radicals; for example, 2,4-dimethyl-4-methylhydroperoxyl-pent-2-yl radical decomposes producing tetramethyl-tetrahydrofuran and an hydroxyl radical. C_8 cyclic ethers are formed in much higher concentrations at 640 K than at 820 K because C_8 alkyl radical β-scission dominates at the higher temperature, also explaining why C_3 and C_4 cyclic ethers exist in higher concentrations than C_8 ethers at 820 K.

C_4 oxygenates are formed from the decomposition of C_8 hydroperoxy-alkyl species and stable ketohydroperoxide species as part of the low-temperature mechanism. They are not formed from isobutene oxidation except for methacrolein, almost half of which is formed from the methallyl radical reaction with $H\dot{O}_2$ radical to form methalloxyl and hydroxyl radicals.

Of the ketones, acetone is measured in the Leppard engine experiments in greatest abundance, Table 3, and is predicted in high concentrations by the model. At 640 K, it is formed via ketohydroperoxide decomposition, addition of the $t\dot{C}_3H_6CHO$ radical to O_2, and tert-butoxy radical decomposition. At 820 K, acetone is mainly a product of isobutene oxidation, another example of the importance of the isobutene submechanism in iso-octane oxidation.

Formaldehyde is also produced in high concentrations. At 640 K, it is produced mainly via $CH_3O_2H = CH_3\dot{O} + \dot{O}H$, followed by $CH_3\dot{O} + O_2 = CH_2O + H\dot{O}_2$. At 820 K, formaldehyde is formed mainly by the reaction of methyl radical with hydroperoxy radical to form methoxy, which decomposes to formaldehyde and H atom as described earlier.

Conclusions

A detailed chemical kinetic model has been assembled to simulate autoignition and intermediate product formation for the primary reference fuels and their mixtures under typical automotive engine conditions. Three sets of experimental results were used to validate the predictive capabilities of the kinetic mechanism. Autoignition delay times measured in a shock tube [13] were simulated with good agreement between model and experiment. Experiments carried out in a high-pressure flow reactor [45] were used, not only to validate the correct overall reactivity but also to identify and calculate the relative distribution of intermediate species produced. These data were supplemented by the experiments of Leppard [20], who differentiated and

quantified the intermediate species produced during PRF oxidation in a motored engine. The major species observed in the experiment are also predicted by the kinetic mechanism. The reaction pathways leading to the major intermediate species in the flow reactor were identified. In addition, we have found that β-scission of octyl radicals occurs at relatively low temperatures' a phenomenon not observed for *n*-heptyl radicals.

REFERENCES

1. Wu, K. C. and Hochgreb, S., *Combust. Flame* 107:383–400 (1996).
2. Eng, J. A., Leppard, W. R., Najt, P. M., and Dryer, F. L., SAE paper 97-2888.
3. Dec, J. E., SAE paper 97-0873.
4. Barnard, J. A. and Harwood, B. A., *Combust. Flame* 21:345–354 (1973).
5. Dryer, F. L. and Brezinsky, K., *Combust. Sci. Technol.* 45:199–212 (1986).
6. Callahan, C. V., Held, T. J., Dryer, F. L., Minetti, R., Ribaucour, M., Sochet, L. R., Faravelli, T., Gaffuri, P., and Ranzi, E., in *Twenty-Sixth Symposium (International) on Combustion,* The Combustion Institute, Pittsburgh, 1996, pp. 739–746.
7. Lignola, P. G., Di Maio, F. P., Marzocchiella, A., Mercogliano, R., and Reverchon, E., in *Twenty-Second Symposium (International) on Combustion,* The Combustion Institute, Pittsburgh, 1988, pp. 1625–1633.
8. D'Anna, A., Mercogliano, R., Barbella, R., and Ciajolo, A., *Combust. Sci. Technol.* 83:217–232 (1992).
9. Ciajolo, A., D'Anna, A., and Mercogliano, R., *Combust. Sci. Technol.* 90:357–371 (1993).
10. Dagaut, P., Reuillon, M., and Cathonnet, M., *Combust. Sci. Technol.* 95:233–260 (1994).
11. Dagaut, P., Reuillon, M., and Cathonnet, M., *Combust. Sci. Technol.* 103:315–336 (1994).
12. Fieweger, K., Blumenthal, R., and Adomeit, G., in *Twenty-Second Symposium (International) on Combustion,* The Combustion Institute, Pittsburgh, 1984, pp. 1579–1585.
13. Fieweger, K., Blumenthal, R., and Adomeit, G., *Combust. Flame* 109:599–619 (1997).
14. Halstead, M. P., Kirsch, L. J., and Quinn, C. P., *Combust. Flame* 30:45–60 (1977).
15. Park, P. and Keck, J. C., SAE paper 90-0027.
16. Griffiths, J. F., Halford-Maw, P. A., and Rose, D. J., *Combust. Flame* 95:291–306 (1993).
17. Minetti, R., Carlier, M., Ribaucour, M., Therssen, E.,

and Sochet, L. R., *Combust. Flame* 102:298–309 (1995).

18. Minetti, R., Carlier, M., and Sochet, L. R., *Combust. Sci. Technol.* 113–114:179 (1996).

19. Minetti, R., Carlier, M., Ribaucour, M., Therssen, E., and Sochet, L. R., in *Twenty-Second Symposium (International) on Combustion,* The Combustion Institute, Pittsburgh, 1996, pp. 747–753.

20. Leppard, W. R., SAE paper 92-2325.

21. Filipe, D. J., Li, H. L., and Miller, D. L., SAE paper 92-0807.

22. Li, H. L., Prabhu, S. K., Miller, D. L., and Cernansky, N. P., SAE paper 94-2062.

23. Ranzi, E., Gaffuri, P., Faravelli, T., and Dagaut, P., *Combust. Flame* 103:91–106 (1995).

24. Ranzi, E., Faravelli, T., Gaffuri, P., Sogaro, A., D'Anna, A., and Ciajola, A., *Combust. Flame* 108:24–42 (1997).

25. Côme, G. M., Warth, V., Glaude, P. A., Fournet, R., Battin-LeClerc, F., and Scacchi, G., in *Twenty-Sixth Symposium (International) on Combustion,* The Combustion Institute, Pittsburgh, 1996, pp. 755–762.

26. Glaude, P. A., Warth, V., Fournet, R., Battin-LeClerc, F., Côme, G. M., and Scacchi, G., *Bull. Soc. Chim. Belg.* 106:343–348 (1997).

27. Roberts, C. E., Matthews, R. D., and Leppard, W. R., SAE paper 96-2107.

28. Chevalier, C., Warnatz, J., and Melenk, H., *Ber. Bunsen-Ges. Phys. Chem.* 94:1362–1367 (1990).

29. Chevalier, C., Pitz, W. J., Warnatz, J., Westbrook, C. K., and Melenk, H., in *Twenty-Fourth Symposium (International) on Combustion,* The Combustion Institute, Pittsburgh, 1992, pp. 92–101.

30. Nehse, M., Warnatz, J., and Chevalier, C., in *Twenty-Sixth Symposium (International) on Combustion,* The Combustion Institute, Pittsburgh, 1996, pp. 773–780.

31. Lund, C. M. and Chase, L., "HCT—A General Computer Program for Calculating Time-Dependent Phenomena Involving One-Dimensional Hydrodynamics, Transport, and Detailed Chemical Kinetics," Lawrence Livermore National Laboratory report UCRL-52504, revised, 1995.

32. Westbrook, C. K. and Pitz, W. J., *Combust. Sci. Technol.* 37:117 (1984).

33. Westbrook, C. K., Warnatz, J., and Pitz, W. J., in *Twenty-Second Symposium (International) on Combustion,* The Combustion Institute, Pittsburgh, 1988, pp. 893–901.

34. Westbrook, C. K., Pitz, W. J., and Leppard, W. R., SAE paper 91-2314.

35. Westbrook, C. K. and Pitz, W. J., WSSCI paper 93-011, Western States Section/The Combustion Institute Meeting, 1993.

36. Curran, H. J., Gaffuri, P., Pitz, W. J., Westbrook, C. K., and Leppard, W. R., SAE paper 95-2406.

37. Curran, H. J., Gaffuri, P., Pitz, W. J., Westbrook, C. K., Callahan, C., Dryer, F. L., and Held, T., in Joint Technical Meeting of the Central States/Western States/Mexican National Sections, The Combustion Institute, San Antonio, TX, 1995, p. 263.

38. Curran, H. J., Pitz, W. J., Westbrook, C. K., Hisham, M. W. M., and Walker, R. W., in *Twenty-Sixth Symposium (International) on Combustion,* The Combustion Institute, Pittsburgh, 1996, pp. 641–649.

39. Curran, H. J., Gaffuri, P., Pitz, W. J., Westbrook, C. K., and Leppard, W. R., in *Twenty-Sixth Symposium (International) on Combustion,* The Combustion Institute, Pittsburgh, 1996, pp. 2669–2677.

40. Curran, H. J., Gaffuri, P., Pitz, W. J., and Westbrook, C. K., *Combust. Flame* 114:149–177 (1998).

41. Ritter, E. R. and Bozzelli, J. W., *Int. J. Chem. Kinet.* 23:767–778 (1991).

42. Benson, S. W., *Thermochemical Kinetics,* Wiley, New York, 1976.

43. Lay, T., Bozzelli, J. W., Dean, A. M., and Ritter, E. R., *J. Phys. Chem.* 99:14514–14527 (1995).

44. Held, T. J., Callahan, C. V., and Dryer, F. L., in The Annual Automotive Technology Development Contractor's Meeting, Dearborn, MI, 1994, p. 257.

45. Callahan, C. V., M. S. E. thesis, Department of Mechanical and Aerospace Engineering, Princeton University, 1995.

46. Held, T. J. and Dryer, F. L., in *Twenty-Fifth Symposium (International) on Combustion,* The Combustion Institute, Pittsburgh, 1994, pp. 901–908.

47. Kim, T. J., Yetter, R. A., and Dryer, F. L., in *Twenty-Fifth Symposium (International) on Combustion,* The Combustion Institute, Pittsburgh, 1994, p. 759.

48. Blin-Simiand, N., Rigny, R., Viossat, V., Circan, S., and Sahetchian, K., *Combust. Sci. Technol.* 88:329–348 (1993).

49. Sahetchian, K. A., Rigny, R., and Circan, S., *Combust. Flame* 85:511–514 (1991).

50. Lee, G. R. and Morley, C., SAE paper 94-1958.

COMMENTS

P. Cadman, University of Wales Aberystwyth, UK. You showed comparisons between your model and the experimental results of Adomeit in a shock tube. I presume that you compared your results with the ignition delays of the pressure rise. How does your model compare and predict the other ignition delays found by Adomeit, for example, those based upon light emission? And the presence of cool flames? He also quotes what he defines as

deflagration to detonation transition. Can you predict these?

Author's Reply. Over a range of initial temperatures of 700–830 K, the experimental results show a two-stage ignition that is also seen in the simulated temperature history. The computed temperature is initially flat followed by a rapid temperature rise of 100–200 K. This temperature rise

is designated the first-stage ignition. Subsequently, the temperature rises slowly until finally a rapid temperature rise occurs signaling a hot (or second stage) ignition. A good illustration of this phenomenon is presented in Fig. 9 of Ref. [40] in this paper. In that study, we compared the time of the first ignition stage reported in a rapid compression machine to the time of the first, modest temperature rise in the model. We also compared the total ignition delay time to the final rapid temperature rise in the model. We followed that same procedure in this study but were unable to show a comparison of the first-stage ignition times due to space limitations. Although we did not publish the comparison of the measured and calculated first-stage ignition times, both the n-heptane and iso-octane models are able to accurately reproduce them.

Our zero-dimensional numerical model cannot predict deflagration-to-detonation transition as it assumes a homogeneous charge. Fieweger et al. (Ref. [13] in the paper) states that the observed deflagration is an inhomogeneous ignition. In order to predict a deflagration-to-detonation transition, one would need a multidimensional model that can treat chemistry, turbulence, turbulent–chemistry interactions, and high-mach number flows. Our understanding of research in this area is that current multi-dimensional models have only a limited ability to predict deflagration-to-detonation transition.